Title
Exposure to Ionizing Radiation Causes Endoplasmic Reticulum Stress in the Mouse Hippocampus.

Journal
Radiation Research, 190(5)

Authors
Hinzman, Charles
Mehta, Khyati
Gill, Kirandeep
et al.

Publication Date
2018-11-01

DOI
10.1667/RR15061.1

Peer reviewed

Published in final edited form as:

Radiat Res. 2018 November ; 190(5): 483–493. doi:10.1667/RR15061.1.

Exposure to Ionizing Radiation Causes Endoplasmic Reticulum Stress in the Mouse Hippocampus

Charles P. Hinzman[a,1], **Janet E. Baulch**[c,1], **Khyati Y. Mehta**[b], **Kirandeep Gill**[b], **Charles L. Limoli**[c], **Amrita K. Cheema**[a,b,2]

[a]Department of Biochemistry, Molecular and Cellular Biology

[b]Department of Oncology, Lombardi Comprehensive Cancer Center, Georgetown University Medical Center, Washington, DC 20057

[c]Department of Radiation Oncology, University of California, Irvine, California 92697

Abstract

It is well known that ionizing radiation-induced toxicity to normal tissue has functional consequences in the brain. However, the underlying molecular alterations have yet to be elucidated. We have previously reported cognitive impairments with concomitant changes in dendritic complexity, spine density and inflammation in mice at 6–24 weeks postirradiation. The goal of this study was to determine whether metabolic changes in the mouse hippocampus after whole-body (4 Gy) or cranial (9 Gy) X-ray irradiation might trigger some of the incipient changes contributing to the persisting pathology in the radiation-injured brain. Metabolomic and lipidomic profiling of hippocampal tissue revealed that radiation induced dyslipidemia in mice at two days and two weeks postirradiation. Strikingly, significant changes were also observed in metabolites of the hexosamine biosynthesis pathway, a finding that was further confirmed using orthogonal methodologies. We hypothesize that these changes in hexosamine metabolism could induce endoplasmic reticulum stress and contribute to radiation-induced cognitive impairments. Taken together, our results show that molecular phenotyping is a valuable approach to identify potentially detrimental pathway perturbations that manifest significantly earlier than gross structural and functional changes in the irradiated brain.

INTRODUCTION

Exposure to ionizing radiation has been shown to induce significant effects on brain structure and function (1). Cognitive impairments are an unintended adverse side effect of clinically relevant radiation treatments for cancers of the central nervous system (CNS) and secondary malignancies in the brain (2, 3). While these persistent, and progressive, effects of radiation have been well documented, the underlying molecular and cellular mechanisms are not clear. Changes to the irradiated brain include depletion of CNS stem cell populations (4,

[2]Address for correspondence: Department of Oncology, GCD-7N Pre-Clinical Science Building, Georgetown University Medical Center, 3900 Reservoir Road NW, Washington, DC 20057; akc27@georgetown.edu.

[1]These authors contributed equally to this work.

Editor's note. The online version of this article (DOI:10.1667/RR15061.1) contains supplementary information that is available to all authorized users.

5) accompanied by reductions in dendritic complexity and spine density (1, 6). These structural and cellular changes translate into significant deficits in short- and long-term learning and memory function that persist with little to no resolution (7). In addition to structural changes, radiation exposure initiates cyclical cascades of secondary reactive processes that involve oxidative stress and inflammation (8–11), processes that serve to perpetuate the signature of radiation injury over time. Collectively, these factors compromise CNS functionality, but definitive links between early and late radiation-induced changes in the CNS have confounded efforts to elucidate the underlying molecular mechanisms.

Previously, we have reported on metabolomic and lipidomic alterations in intestinal and liver tissue injury in mice that received sublethal-dose whole-body irradiation. In this study, we used a high-resolution mass spectrometry approach for analyzing hippocampal tissue obtained from mice that received cranial (9 Gy) or whole-body (4 Gy) X-ray irradiation. The tissue samples from sham or irradiated mice were collected at two days or two weeks postirradiation (Fig. 1). Our data indicate that mice receiving whole-body or cranial irradiation undergo dyslipidemia in the mouse hippocampus. Furthermore, hippocampal tissue metabolomic profiles in cranially irradiated mice exhibit perturbations in metabolites, such as UDP-N-acetylglucos-amine (UDP-GlcNAc), which could be indicative of early onset endoplasmic reticulum (ER) stress that may initiate the types of metabolic perturbations that eventually lead to cognitive impairment over time. Although the brain has typically been considered a late-responding organ to radiation exposure, this study demonstrates that whole-body irradiation (4 Gy) induces detrimental metabolic consequences in hippocampus that manifest as early as 48 h postirradiation. Some of these changes are persistent and may contribute to structural, cellular and functional impairments that persist and progress over time.

MATERIALS AND METHODS

Animal Housing and Irradiation

All animal procedures described in this study were performed in accordance with NIH guidelines and approved by the University of California Institutional Animal Care and Use Committee. Two-month-old male C57Bl/6J wild-type mice were purchased (Jackson Laboratory, Bar Harbor, ME) and maintained in sterile housing conditions (20°C ± 1°C; 70% ± 10% humidity; 12 h light-dark schedule) with *ad libitum* access to standard rodent chow (Envigo Teklad 2020x) and water. The mice were randomly divided into three experimental groups (n = 16 mice per group): nonirradiated concurrent controls; whole-body irradiation (4 Gy); and head only (cranial) irradiation (9 Gy). Mice were acclimated in the vivarium for approximately two weeks prior to irradiation. For irradiations, mice were anesthetized (5% induction and 2% maintenance isoflurane, vol/vol), placed ventrally and without restraint on the treatment table (X-RAD 320 irradiator; Precision X-ray Inc., North Branford, CT). Cranial irradiations were performed using a collimated beam (1.0 cm^2 diameter) such that the cerebellum, eyes and rest of the body were shielded from exposure. Whole-body irradiations were performed without the collimator. The irradiator was equipped with a hardening filter (0.75 mm tin, 0.25 mm copper and 1.5 mm aluminum; HVL = 3.7 mm copper, half-value layer) to eliminate low-energy X rays and minimize skin

damage. Radiation was delivered at a dose rate of 1.10 Gy min^{-1}. Nonirradiated control mice were placed under anesthesia for 5 min without X-ray exposure. Although food intake was not measured for this study, qualitatively we did not observe any changes. At the selected times of two days or two weeks postirradiation, mice were deeply anesthetized with isoflurane and euthanized using saline with heparin (10 U/ml, intracardiac perfusion; Sigma-Aldrich LLC, St. Louis, MO). Brains were then micro-dissected for hippocampi that were snap frozen using liquid nitrogen.

Hippocampal Tissue Preparation for Mass Spectrometry Analysis

Tissue (5 mg) was homogenized on ice in 500 µl of chilled 50% methanol and 50% water combined, containing internal standards (debrisoquine and 4-nitrobenzoic acid). Samples were then centrifuged at 14,000 rpm for 15 min at 4°C. Supernatant was transferred to fresh tubes and combined with a 1:1 volume of acetonitrile (ACN). Samples were vortexed and incubated on ice for 20 min. Pellets were saved for later use (pellet 1). After incubation, samples were centrifuged at 14,000 rpm for 15 min at 4°C. Supernatant was collected, dried by vacuum and stored in −80°C until use (SN1). The second pellet was saved (pellet 2). Pellets 1 and 2 were each resuspended in 250 µl of chilled 3:1 dichloromethane:methanol and combined into a new tube. Samples were then sonicated for 90 s in an ice bath and centrifuged for 15 min at 4°C, 14,000 rpm. Supernatant was placed in a fresh tube with 1:1 volume of ACN, vortexed and incubated on ice for 20 min. Pellet (pellet 3) was saved at −80°C for protein quantification via Bradford assay. Samples were again centrifuged at 14,000 rpm for 15 min at 4°C. This supernatant was then collected, dried by vacuum and stored at −80°C until use (SN2). Supernatants SN1 and SN2 were reconstituted in 200 µl of 50% methanol, 25% ACN and 25% water combined, just prior to loading into vials for UPLC-ESI-Q-TOF-MS analysis. Quality control (QC) samples were prepared by pooling 2 µl of each sample.

Hippocampal Tissue Analysis Using UHPLC-Q-TOF Mass Spectrometry

For metabolomics analysis, each sample (2 µl) was injected onto a reverse-phase 100 × 2.1 mm ACQUITY 1.8-µm HHS T3 column at 45°C column temperature (Waters Corp., Milford, MA) using an ACQUITY UHPLC system (Waters Corp.) with a gradient mobile phase consisting of 100% water containing 0.1% formic acid (solvent A) and 100% methanol containing 0.1% formic acid (solvent B) and resolved for 13 min at a flow rate of 0.4 ml/min. The gradient started with 98% solvent A and 2% solvent B for 0.5 min with a ramp of curve 6. At 5 min, the gradient reached 95% solvent A and 5% solvent B. At 7.5 min, the gradient shifted to 10% solvent A and 90% solvent B for 1 min. At 11.50 min, it reached initial conditions and continued to the end of the run.

For lipidomics analysis, samples were run on a reverse-phase 100 × 2.1 mm ACQUITY 1.7-µm CSH C18 column (Waters Corp.) at a column temperature of 65°C. The run time was 11 min at a flow rate of 0.45 ml/min. The gradient included two solvents: 50% ACN and 50% water with 0.1% formic acid and 10 m*M* ammonium formate (solvent A); and 90% IPA and 10% ACN containing 0.1% formic acid and 10 m*M* ammonium formate (solvent B). The gradient started with 60% solvent A and 40% solvent B with a ramp of curve 6 for 0.5 min.

At 8 min, the gradient reached 100% solvent B. At 9 min, the gradient returned to initial conditions until the end of the run.

The column eluent was introduced directly into the mass spectrometer by electrospray. Mass spectrometry was performed on a Q-TOF MS (Xevo G2-S QTOF MS; Waters Corp.), operating in either negative-ion (ESI^-) or positive-ion (ESI^+) electrospray ionization mode with a capillary voltage of 3 kV for positive mode and 2.75 kV for negative mode and a sampling cone voltage of 30 V in the positive mode and 20 V in the negative mode. The source offset for negative mode was at 80. The desolvation gas flow was set to 600 liters/h and the temperature was set to 500°C. The cone gas flow was 25 liters/h, and the source temperature was 100°C. Accurate mass was maintained by introduction of LockSpray™ interface of leucine enkephalin [556.2771 $(M + H)^+$ or 554.2615 $(M – H)^-$] at a concentration of 1 ng/μl in 50% aqueous ACN and a rate of 5 μl/min. Data were acquired in centroid mode from 50 to 1,200 m/z in MS scanning. Pooled QC samples were run at the beginning of the run for column conditioning, thereafter every 10 samples, and at the end of the run to monitor data reproducibility. For internal standards, we calculated the following coefficient of variations (CV) for the QC samples across columns and ionization modes: metabolomics positive = 10.33%; metabolomics negative = 18.9%; lipidomics positive = 10.36%; and lipidomics negative = 6.8%. We then generated QC overlay chromatograms to measure retention time shifts (Supplementary Fig. S1; http://dx.doi.org/10.1667/RR15061.LS1). MetMix, an external standard cocktail including acetaminophen, sulfaguanidine, sulfadimethoxine, val-tyr-val, terfenadine and leucine-enkaphalin, was tested before and after each run. PPM errors chromatograms have been included for lipidomics and metabolomics (Supplementary Table S1).

Liquid Chromatography-Mass Spectrometry (LC-MS) Data Processing and Statistical Analysis

Mass spectrometry data from the UHPLC-Q-TOF-MS were processed using R software package “xcms” (Scripps Institute, LaJolla, CA) generating a data matrix containing ion intensities, mass to charge (m/z) and retention time values. Data were normalized to the intensities of internal standards and concentration of protein in each hippocampal tissue sample as determined by Bradford assay. Multivariate statistical analyses were performed using Metaboanalyst version 3.0 (Xia laboratory, McGill University, Montreal Canada) with log transformation and Pareto scaling. Binary comparisons were performed for each time point using Student’s two-tailed t test with homogenous variance, considering $P < 0.05$ to identify significant m/z values. Partial least squares discriminant analysis (PLS-DA) was performed using all identified features, to measure separation between groups. Significantly dysregulated metabolites and lipids were annotated using tandem mass spectrometry and SimLipid software version 6.01 (PREMIER Biosoft International, Palo Alto, CA) using fragmentation pattern matching, respectively. Figures were generated using Metaboanalyst version 3.0, GraphPad Prism 7 (LaJolla, CA) and in-house R scripts.

Hippocampal Tissue Real-Time Reverse Transcriptase PCR (RT-qPCR) Array Analysis

Mice (n = 4 per group) were randomly chosen for RT-qPCR analysis. RNA was isolated from hippocampal tissue samples using an RNeasy lipid tissue extraction kit (QIAGEN,

Germantown, MD) according to manufacturer's protocol and tested for concentration and purity using a NanoDrop spectrophotometer (Thermo Fisher Scien tific™, Waltham, MA). cDNA was synthesized using the RT^2 First Strand Kit (QIAGEN) according to manufacturer's protocol. RT^2 PCR 384-well arrays were purchased (QIAGEN) to test samples for gene expression changes in the unfolded protein response. Three samples per plate were loaded (one each of a sham, 4 Gy and 9 Gy irradiated mouse) according to manufacturer protocol, with RT^2 SYBR Green ROX qPCR Master Mix (QIAGEN), using four plates for the 12 samples. Plates were run on a QuantStudio 12k Flex Real-Time PCR instrument (Thermo Fisher Scientific), and gene expression and statistical analysis was performed with Thermo Fisher Cloud relative quantification software using the ΔΔCt method (Thermo Fisher Scientific). Experiments were performed in triplicate and Student's two-tailed *t* test with homogeneous variance was used to compare gene expression across each irradiated group to control, with $P < 0.05$ considered significant.

Lipid Peroxidation Assay

Malondialdehyde (MDA), an end product of lipid peroxidation, forms an adduct with thiobarbituric acid (TBARS) at 90–100°C leading to a colorimetric change that can be measured at 540 nm using a microplate reader (Synergy Mx; BioTek Instruments Inc., Winooski, VT). Levels of MDA were measured in hippocampal lysates using the TBARS Assay Kit (Cayman Chemical, Ann Arbor, MI) according to the manufacturer's protocol. Results were corrected for protein level and reported in μ*M* MDA/μg protein. Two-tailed *t* tests were used to compare MDA levels in each irradiated group [two-day (4 Gy and 9 Gy), two-week (4 Gy and 9 Gy)] to their respective sham-irradiated group.

RESULTS

Ionizing Radiation Induces Dyslipidemia in the Mouse Hippocampus

To investigate the effect of whole-body and/or cranial irradiation on the hippocampus, we performed comparative metabolomic and lipidomic profiling of tissue obtained from wild-type mice at two days and two weeks after 4 Gy whole-body irradiation or 9 Gy cranial irradiation (Fig. 1), using UHPLC-Q-TOF-MS. Beginning with no underlying assumptions, our goal was to recapitulate changes in metabolomic and lipidomic profiles due to exposure in two scenarios. We chose a 9 Gy localized cranial dose to model the clinical management of CNS malignancies. However, 9 Gy whole-body irradiation would result in significant lethality. For this reason, we selected a 4 Gy whole-body dose, to be more representative of an unintended exposure scenario, with an increased likelihood of survival. In an attempt to gauge the similarities, or differences, in the acute radioresponse of these two scenarios, we chose time points of two days and two weeks postirradiation. By selecting these doses and time points, the resultant changes in metabolomic profiles could elucidate both the contrasting and common radioresponsive path-ways.

Preprocessing of LC-MS data using XCMS resulted in a total of 4,146 features in ESI$^+$ mode and 4,808 features in the ESI$^+$ mode, across metabolomics and lipidomics analyses, which were subjected to multivariate analyses. Separation of goods using principal component analysis was not satisfactory. Therefore, we chose to proceed using PLS-DA to

measure group separation, an approach used by our group and others for radiation metabolomics studies (12). PLS-DA resulted in clear separation of groups of mice that received radiation exposures from those that were sham irradiated (Fig. 2A, Supplementary Figs. S2 and S3; http://dx.doi.org/10.1667/RR15061.1.S1) with $R^2 = 0.83$ and $Q^2 = 0.15$ across 3 components. Putative markers were selected by examining the volcano plot and considering a fold-change threshold of >1.8 or <0.5 and $P < 0.05$ (Fig. 2B). After performing binary comparisons for each group (2 day, controls vs. 2 day, 4 Gy; 2 day, controls vs. 2 day, 9 Gy; 2 week, controls vs. 2 week, 4 Gy; and 2 week, controls vs. 2 week, 9 Gy) using a two-tailed Student's *t* test with equal variance, we found 1,608 and 1,279 features that were statistically significantly dysregulated in our metabolomics and lipidomics study, respectively. A total of 83 metabolites were annotated using tandem mass spectrometry and fragmentation pattern matching using SimLipid software (Supplementary Table S2). Several major classes of glycerophospholipids, including phosphatidylcholine, phosphatidylinositol, phosphatidylserine and phosphatidylethanolamine, were significantly downregulated after irradiation (Fig. 3A). We also observed significant downregulation of sphingomyelin at two weeks postirradiation. At two days after 4 Gy irradiation, 9 PCs and 1 PE were significantly dysregulated. At two weeks after 4 Gy irradiation, we observed a decrease in 11 PCs, 6 PEs, 2 PGs, 4 PIs, 1 PS and 3 SMs. At two weeks after 9 Gy cranial irradiation, we found dysregulation in 17 PCs, 8 PEs, 1 PG, 3 PIs, 2 PSs and 5 SMs. Interestingly, dyslipidemia was more apparent at two weeks postirradiation, suggesting a systemic late effect. Additionally, the two-week lipidomic profiles of mice receiving whole-body irradiation corroborated the profiles of those mice that received cranial irradiation at that same time, suggesting susceptibility of the hippocampus to a radiation response at comparatively lower whole-body radiation doses. This is a striking finding since the brain has generally been considered relatively insensitive to radiation compared to other organ sites (13), although a few cGy of space radiation has been found to induce long-lasting changes in rodent behavior.

However, this dysregulation did not apply to all classes of lipids. We observed a number of lipid classes, including fatty acids, phosphatidic acids, lysobisphosphatidic acids and lysophosphatidylethanolamines, which were not significantly dysregulated (unpublished data). To investigate the cause of dyslipidemia we performed a lipid peroxidation assay. MDA is a well-known product of lipid peroxidation, a mechanism of cellular stress induced and sustained by oxidative stress, which can be measured using the TBARS assay (14, 15). We found increased MDA levels at two days after 4 Gy whole-body and 9 Gy cranial irradiation, suggesting increased levels of lipid peroxidation at early postirradiation times (Fig. 3B). Interestingly, we observed that by two weeks postirradiation, lipid peroxidation was no longer significantly upregulated compared to sham-irradiated mice, indicating that lipid peroxidation is likely an acute response to radiation damage that dissipates over time (Fig. 3C). Given this result, lipid peroxidation could contribute to dyslipidemia right after irradiation, but is unlikely to be the primary driver of persistent lipid dysregulation two weeks after irradiation.

Next, we investigated the commonalities in hippocampus metabolomic/lipidomic profiles between whole-body and cranially irradiated mice. Initially we looked for metabolites that were shared between the two exposure groups. Strikingly, we found a number of lipids that

were dysregulated in both the two-day whole-body irradiation group (4 Gy) and the two-week cranial irradiation group (9 Gy) (Fig. 4A). This finding indicates that even short-term whole-body radiation exposure can result in dyslipidemia in a manner similar to a higher dose exposure to the brain alone.

As described above, we observed a similar pattern of dyslipidemia in hippocampal tissue at 2 weeks after whole-body irradiation as well as after cranial irradiation. Figure 4B shows box and whisker plots of specific metabolites that were dysregulated in both groups. We found all of these lipids to be downregulated, except for PI (22:4/16:0). This phosphatidylinositol was found to be significantly upregulated in both two-week postirradiation groups. The biological significance of this lipid is still under investigation; however, it could potentially serve as a biomarker for radiation damage in hippocampal tissue.

Cranial Radiation Exposure May Cause Endoplasmic Reticulum Stress in the Brain

To our knowledge, the metabolic consequences of radiation-induced injury to hippocampal tissue have not been previously studied. Therefore, we next investigated dysregulation of biochemical pathways specific to the two-week cranial irradiation cohort (9 Gy, head only). We began by examining the separation in this group using a PLS-DA plot (Fig. 5A) which demonstrated clear separation between groups with $R^2 = 0.905$ and $Q^2 = -0.07$ across three components. In this cohort, we validated a number of metabolites that showed differential abundance in the irradiated mice compared to sham-irradiated mice. Those metabolites included oxidized glutathione, glycerophosphocholine, guanosine monophosphate (GMP), UDP-glucose and UDP-GlcNac, all of which were significantly upregulated compared to controls (Fig. 5B). Although these markers have been linked to various stresses (16–18), UDP-GlcNac was particularly interesting since it is the final product of the hexosamine biosynthesis pathway (HBP) that has been previously linked to ER stress in astrocytes (19).

Therefore, to determine whether our findings from metabolite profiling correlated with increased ER stress in the hippocampus, we performed RT-qPCR to measure changes in known genetic markers of ER stress (20–26). We discovered a number of ER stress-associated genes that were significantly changed in the two-week 9 Gy cranially irradiated group, including CCAAT/enhancer-binding protein, beta (CEBPB), ring finger protein 139 (RNF139), prefoldin 2 (PFDN2), mitogen-activated protein kinase 9 (MAPK9, JNK2), DNAJ heat-shock protein family (HSP40) member B2 (DNAJB2), membrane-bound transcription factor peptidase, site 1 (MBTPS1) and cAMP responsive element binding protein 3 (CREB3) (Fig. 6). Results for all genes tested in the array can be found in Supplementary Table S3 (http://dx.doi.org/10.1667/RR15061.1.S1). These data suggest that early changes in ER stress may operate to perturb CNS signaling and synaptic transmission, although this currently remains speculative.

DISCUSSION

To the best of our knowledge, this is the first published study that describes the effects of ionizing radiation on the metabolomic and lipidomic profiles of the mouse hippocampus using LC-MS. Here we report that mice receiving either 4 Gy whole-body or 9 Gy cranial

X-ray irradiation experience significant dyslipidemia. Previously published findings have shown that whole-body irradiation can result in significant lipid dysregulation (27–29). Surprisingly, however, we found that as early as two days after 4 Gy whole-body irradiation, the hippocampus exhibited lipid dysregulation in a manner similar to that observed in mice two weeks after 9 Gy cranial irradiation. A rather simplistic interpretation of this result may lie in the fact that many early responding tissues with increased proliferation rates were exposed at 4 Gy, while the late responding tissue with much slower rates of proliferation exhibited a corresponding delayed dysregulation after the higher 9 Gy dose. This suggests that systemic changes resulting from whole-body irradiation cause normal tissue toxicity, affecting tissue structure and function, including hippocampus. We also found evidence of increased lipid peroxidation at two days postirradiation. These results suggest that the brain is not as radioresistant as is traditionally believed, and even whole-body acute exposure to ionizing radiation could lead to tissue-level lipid remodeling. While nearly all validated lipids were downregulated after irradiation, one lipid was found to be significantly upregulated: PI (22:4/16:0). The biological relevance of this lipid remains unknown. Given that this phosphatidylinositol was the only lipid found to be upregulated, it could serve as a potential marker for radiation-induced tissue damage to the brain. Downregulation of a broad class of lipids in hippocampal tissue in response to radiation is an interesting finding; it is likely that lipid mediators of inflammation may be readily assayable in bodily fluids rather than at the local tissue level where metabolites related to structural and functional changes would be more apparent. Our follow-up studies with plasma and plasma exosomes from the same mouse cohort may help provide better insights into this initial observation.

Interestingly, in the two-week cranial (9 Gy) irradiation group, we identified a number of metabolites, including oxidized glutathione, GMP, UDP-glucose and UDP-GlcNAc, which were significantly upregulated. Oxidized glutathione is a well-known marker of oxidative stress (16, 17). UDP-glucose has been shown to stimulate oligodendrocyte precursors in response to various tissue stress and trauma (18). UDP-GlcNac is the final product in the HBP. In tandem with increased oxidative stress, increased levels of UDP-GlcNac indicate elevated HBP flux (30). Taken together, the upregulation of these metabolites could be indicative of various stress events, including increased oxidative stress, HBP flux and ER stress. Importantly, we validated increased ER stress in the hippocampal tissue samples obtained from the same cohort of mice, using RT-qPCR, and discovered significant dysregulation of a number of genes, including CEBPB, RNF139, PFDN2, MAPK9 (JNK2), DNAJB2, MBTPS1 and CREB3, known to be involved in ER function and stress signaling (20−26). The culmination of these results is shown in Fig. 7. Radiation-induced damage results in higher levels of intracellular ROS, leading to increased oxidative stress in the hippocampus. Increased oxidative stress results in acute lipid peroxidation, long-term dyslipidemia and increased HBP flux. Aberrant levels of UDP-GlcNac through the HBP pathway likely result in ER stress, representing a potentially new pathway that could contribute to the onset and development of cognitive impairment after cranial and/or whole-body irradiation.

Localized cranial exposure has been shown to result in significant neurocognitive dysfunction (31–35); metabolic profiling, performed at early time points postirradiation, helped identify metabolic pathways that may contribute to cognitive impairment over time.

While behavioral studies typically do not detect cognitive effects until 6–12 weeks postirradiation, the metabolomics profiling approach used in this study enabled the detection of metabolic perturbations as early as two days postirradiation, thus underscoring the power of molecular phenotyping studies (36–38). To date, published studies have shown that a variety of other factors can influence radiation-induced cognitive dysfunction, including damage to the microvasculature and inhibition of microglial activation (33, 34). Although, the mechanisms by which cognition is impaired are multifaceted and incompletely understood, ER stress has been implicated in the induction of cognitive impairments in studies using rats (39), albeit in the absence of radiation. Nonetheless, we have identified novel mechanisms, including increased HBP flux and ER stress, which could also contribute to radiation-induced cognitive impairment. Importantly, we demonstrate the utility of LC-MS as a method for better understanding the pathways compromised in the irradiated brain.

Supplementary Material

Refer to Web version on PubMed Central for supplementary material.

ACKNOWLEDGMENTS

This work was supported by the National Institute of Neurological Disorders and Stroke (NINDS grant nos. NS089575 and HDTRA1-13-1-0022 to CL) and the National Institute of Allergy and Infectious Diseases (NIAID grant no. 1U01AI133561-01 to AKC). We also acknowledge the Metabolomics Shared Resource at Georgetown University (Washington, DC), which is partially supported by NIH/NCI/CCSG grant no. P30-CA051008. We thank the anonymous reviewers whose constructive comments helped improve and clarify our manuscript.

REFERENCES

1. Parihar VK, Limoli CL. Cranial irradiation compromises neuronal architecture in the hippocampus. Proc Natl Acad Sci 2013: 110:12822–7. [PubMed: 23858442]
2. Meyers CA. Neurocognitive dysfunction in cancer patients. Oncology (Williston Park) 2000; 14:75–79; discussion 79, 81–72, 85. [PubMed: 10680150]
3. Makale MT, McDonald CR, Hattangadi-Gluth JA, Kesari S. Mechanisms of radiotherapy-associated cognitive disability in patients with brain tumours. Nat Rev Neurol 2016; 13:52–64. [PubMed: 27982041]
4. Mizumatsu S, Monje ML, Morhardt DR, Rola R, Palmer TD, Fike JR. Extreme sensitivity of adult neurogenesis to low doses of extreme sensitivity of adult neurogenesis to low doses of X-irradiation. Cancer Res 2003; 63:4021–7. [PubMed: 12874001]
5. Parihar VK, Acharya MM, Roa DE, Bosch O, Christie L-A, Limoli CL. Defining functional changes in the brain caused by targeted stereotaxic radiosurgery. Transl Cancer Res 2014; 3:124–37. [PubMed: 24904783]
6. Parihar VK, Pasha J, Tran KK, Craver BM, Acharya MM, Limoli CL. Persistent changes in neuronal structure and synaptic plasticity caused by proton irradiation. Brain Struct Funct 2015; 220:1161–71. [PubMed: 24446074]
7. Acharya MM, Martirosian V, Christie L-A, Limoli CL. Long-term cognitive effects of human stem cell transplantation in the irradiated brain. Int J Radiat Biol 2014; 90:816–20. [PubMed: 24882389]
8. Tseng BP, Lan ML, Tran KK, Acharya MM, Giedzinski E, Limoli CL. Characterizing low dose and dose rate effects in rodent and human neural stem cells exposed to proton and gamma irradiation. Redox Biol 2013; 1:153–62. [PubMed: 24024148]
9. Tseng BP, Giedzinski E, Izadi A, Suarez T, Lan ML, Tran KK, et al. Functional consequences of radiation-induced oxidative stress in cultured neural stem cells and the brain exposed to charged particle irradiation. Antioxid Redox Signal 2014; 20:1410–22. [PubMed: 23802883]

10. Acharya MM, Rosi S, Jopson T, Limoli CL. Human neural stem cell transplantation provides long-term restoration of neuronal plasticity in the irradiated hippocampus. Cell Transplant 2015; 24:691–702. [PubMed: 25289634]
11. Acharya MM, Martirosian V, Christie L-A, Riparip L, Strnadel J, Parihar VK, et al. Defining the optimal window for cranial transplantation of human induced pluripotent stem cell-derived cells to ameliorate radiation-induced cognitive impairment. Stem Cells Transl Med 2015; 4:74–83. [PubMed: 25391646]
12. Johnson CH, Patterson AD, Krausz KW, Kalinich JF, Tyburski JB, Kang DW, et al. Radiation metabolomics. 5. Identification of urinary biomarkers of ionizing radiation exposure in nonhuman primates by mass spectrometry-based metabolomics. Radiat Res 2012; 178:328–40 [PubMed: 22954391]
13. Hall EJ, Giaccia A. Radiobiology for the radiologist. 8th ed Philadelphia: Lippincott Williams & Wilkins; 2012
14. Yagi K. Simple assay for the level of total lipid peroxides in serum or plasma. Methods Mol Biol 1998; 108:101–6. [PubMed: 9921519]
15. Armstrong D, Browne R. The analysis of free radicals, lipid peroxides, antioxidant enzymes and compounds related to oxidative stress as applied to the clinical chemistry laboratory. Adv Exp Med Biol 1994; 366:43–58. [PubMed: 7771281]
16. Giustarini D, Dalle-Donne I, Tsikas D, Rossi R. Oxidative stress and human diseases: Origin, link, measurement, mechanisms, and biomarkers. Crit Rev Clin Lab Sci 2009; 46:241–81. [PubMed: 19958214]
17. Dalle-Donne I, Rossi R, Colombo R, Giustarini D, Milzani A. Biomarkers of oxidative damage in human disease. Clin Chem 2006; 52:601–23. [PubMed: 16484333]
18. Coppi E, Maraula G, Fumagalli M, Failli P, Cellai L, Bonfanti E, et al. UDP-glucose enhances outward K(+) currents necessary for cell differentiation and stimulates cell migration by activating the GPR17 receptor in oligodendrocyte precursors. Glia 2013: 61:1155–71. [PubMed: 23640798]
19. Matthews AJ, Belof JL, Acevedo-Duncan M, Potter RL. Glucosamine-induced increase in Akt phosphorylation corresponds to increased endoplasmic reticulum stress in astroglial cells. Mol Cell Biochem 2007; 298:109–23. [PubMed: 17136481]
20. Luan Q, Jin L, Jiang CC, Tay KH, Lai F, Liu XY, et al. RIPK1 regulates survival of human melanoma cells upon endoplasmic reticulum stress through autophagy. Autophagy 2015; 11:975–94. [PubMed: 26018731]
21. Ramos-Lopez O, Riezu-Boj JI, Milagro FI, Martinez JA. DNA methylation signatures at endoplasmic reticulum stress genes are associated with adiposity and insulin resistance. Mol Genet Metab 2018; 123:50–8. [PubMed: 29221916]
22. Yang Y, Lin P, Chen F, Wang A, Lan X, Song Y, et al. Luman recruiting factor regulates endoplasmic reticulum stress in mouse ovarian granulosa cell apoptosis. Theriogenology 2013; 79:633–9.e1–3. [PubMed: 23270862]
23. Brown M, Strudwick N, Suwara M, Sutcliffe LK, Mihai AD, Ali AA, et al. An initial phase of JNK activation inhibits cell death early in the endoplasmic reticulum stress response. J Cell Sci 2016; 129:2317–28. [PubMed: 27122189]
24. Bai Y, Wei Y, Wu L, Wei J, Wang X, Bai Y. C/EBP beta mediates endoplasmic reticulum stress regulated inflammatory response and extracellular matrix degradation in LPS-stimulated human periodontal ligament cells. Int J Mol Sci 2016; 17:1–11.
25. Torres-Odio S, Key J, Hoepken HH, Canet-Pons J, Valek L, Roller B, et al. Progression of pathology in PINK1-deficient mouse brain from splicing via ubiquitination, ER stress, and mitophagy changes to neuroinflammation. J Neuroinflammation 2017; 14:1–26. [PubMed: 28086917]
26. Brandl K, Rutschmann S, Li X, Du X, Xiao N, Schnabl B, et al. Enhanced sensitivity to dss colitis caused by a hypomorphic Mbtps1 mutation disrupting the atf6-driven unfolded protein response. Proc Natl Acad Sci U S A 2009; 106:3300–5. [PubMed: 19202076]
27. Haimovitz-Friedman A, Kan CC, Ehleiter D, Persaud RS, McLoughlin M, Fuks Z, et al. Ionizing radiation acts on cellular membranes to generate ceramide and initiate apoptosis. J Exp Med 1994; 180:525–35. [PubMed: 8046331]

28. Goudarzi M, Weber WM, Chung J, Doyle-Eisele M, Melo DR, Mak TD, et al. Serum dyslipidemia is induced by internal exposure to strontium-90 in mice, lipidomic profiling using a data-independent liquid chromatography-mass spectrometry approach. J Proteome Res 2015; 14:4039–49. [PubMed: 26262552]
29. Miltonprabu S, Thangapandiyan S. Epigallocatechin gallate potentially attenuates Fluoride induced oxidative stress mediated cardiotoxicity and dyslipidemia in rats. J Trace Elem Med Biol 2015; 29:321–35. [PubMed: 25282272]
30. Fantus IG, Goldberg HJ, Whiteside CI, Topic D. The hexosamine biosynthesis pathway In: Cortes P, Mogensen CE, editors. The diabetic kidney. Totowa, NJ: Humana Press; 2006 p. 117–33.
31. Rola R, Raber J, Rizk A, Otsuka S, VandenBerg SR, Morhardt DR, et al. Radiation-induced impairment of hippocampal neurogenesis is associated with cognitive deficits in young mice. Exp Neurol 2004; 188:316–30. [PubMed: 15246832]
32. Greene-Schloesser D, Robbins ME, Peiffer AM, Shaw EG, Wheeler KT, Chan MD. Radiation-induced brain injury: A review. Front Oncol 2012; 2:73. [PubMed: 22833841]
33. Dutta V. Uncomfortable bedfellows: Whole brain radiation therapy and neurocognition in animal and human studies. J Cancer Res Ther 2015; 11:679–83. [PubMed: 26881501]
34. Rana P, Gupta M, Khan AR, Hemanth Kumar BS, Roy R, Khushu S. NMR based metabolomics reveals acute hippocampal metabolic fluctuations during cranial irradiation in murine model. Neuro-chem Int 2014; 74:1–7.
35. Hladik D, Tapio S. Effects of ionizing radiation on the mammalian brain. Mutat Res 2016; 770:219–30. [PubMed: 27919332]
36. Lamproglou I, Chen QM, Boisserie G, Mazeron J-J, Poisson M, Baillet F, et al. Radiation-induced cognitive dysfunction: An experimental model in the old rat. Int J Radiat Oncol 1995; 31:65–70.
37. Kempf SJ, Casciati A, Buratovic S, Janik D, von Toerne C, Ueffing M, et al. The cognitive defects of neonatally irradiated mice are accompanied by changed synaptic plasticity, adult neurogenesis and neuroinflammation. Mol Neurodegener 2014; 9:57. [PubMed: 25515237]
38. Fike JR. Physiopathology of radiation-induced neurotoxicity Pathophysiologie de la neurotoxiciteadio-induite. Rev Neurol (Paris) 2011; 167:746–50. [PubMed: 21889778]
39. Cai F, Liu J, Li C, Wang J. Critical role of endoplasmic reticulum stress in cognitive impairment induced by microcystin-LR. Int J Mol Sci 2015; 16:28077–86. [PubMed: 26602924]

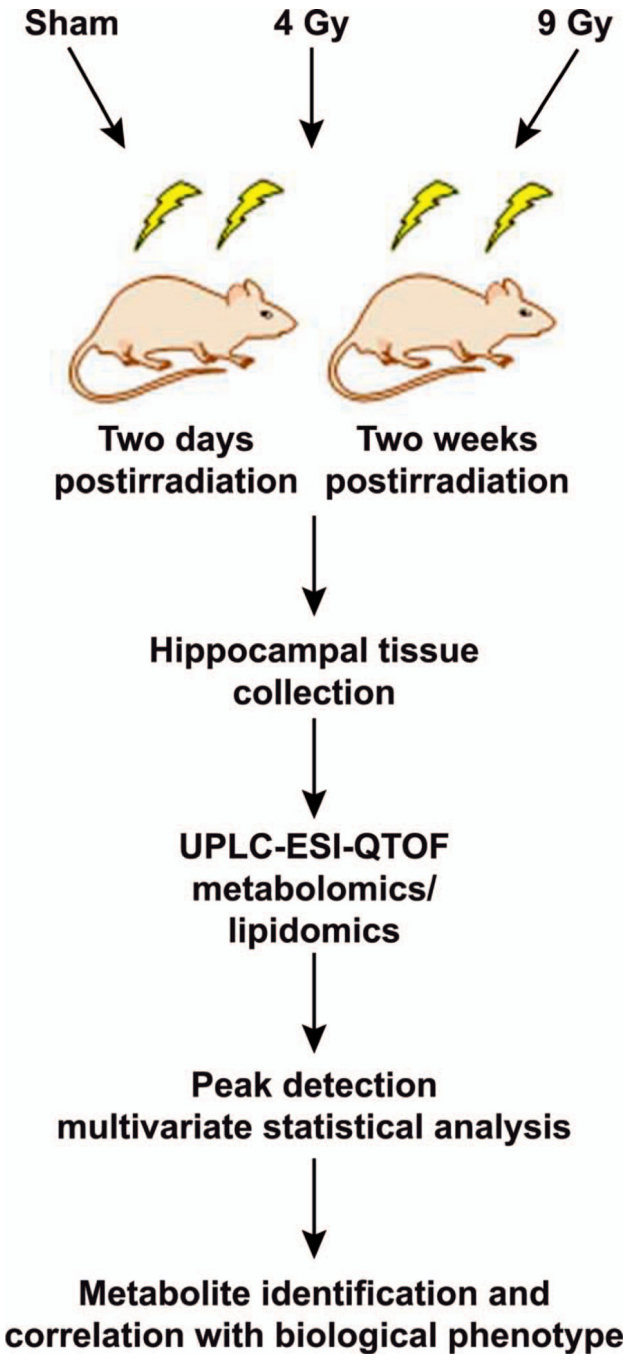

FIG. 1.

Experimental design. Mice received either 4 Gy whole-body or 9 Gy cranial X-ray irradiation or sham irradiation. Radiation was delivered in a single acute dose and hippocampal tissue was collected at two days or two weeks postirradiation. Tissue samples were processed and analyzed via UHPLC-Q-TOF-MS. Detected features were tested for statistical significance, validated by Tandem MS (MS/MS) and investigated for functional significance.

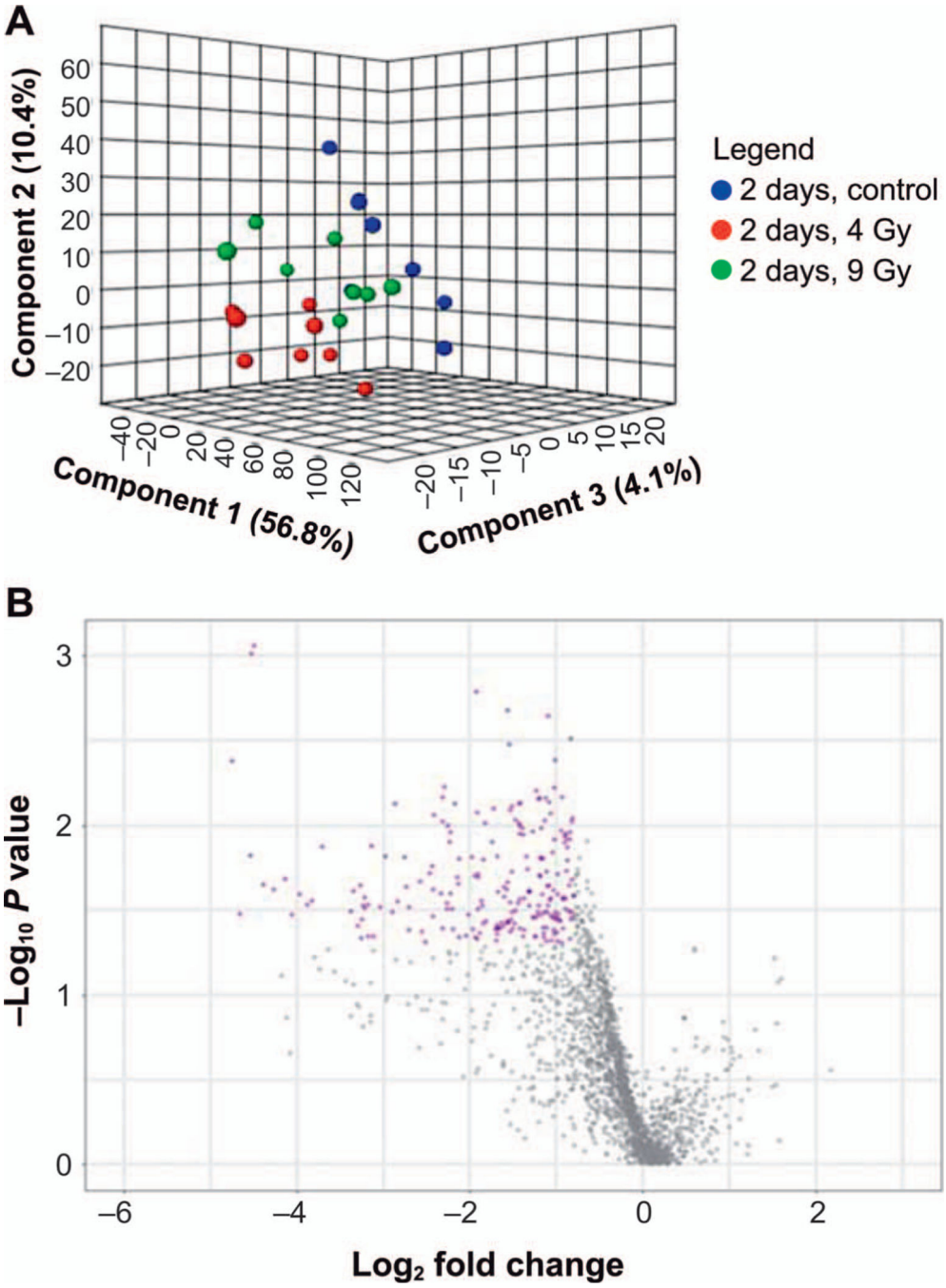

FIG. 2.

Comparative metabolic profiling. Panel A: Partial least squares discriminant analysis (PLS-DA) plot comparing metabolite profiles (all observed features) in hippocampal tissue derived from sham-irradiated mice vs. mice at two days after 4 Gy whole-body or 9 Gy cranial irradiation. Representative data were captured in the metabolomics negative ionization mode. Panel B: Volcano plot capturing fold change vs. statistical significance of change (*P* value). Each purple dot represents putative m/z with $P < 0.05$ and fold change >1.8 or <0.5.

Comparison between two-week control mice and mice at two weeks after 4 Gy whole-body irradiation. Representative data were captured in the metabolomics positive ionization mode.

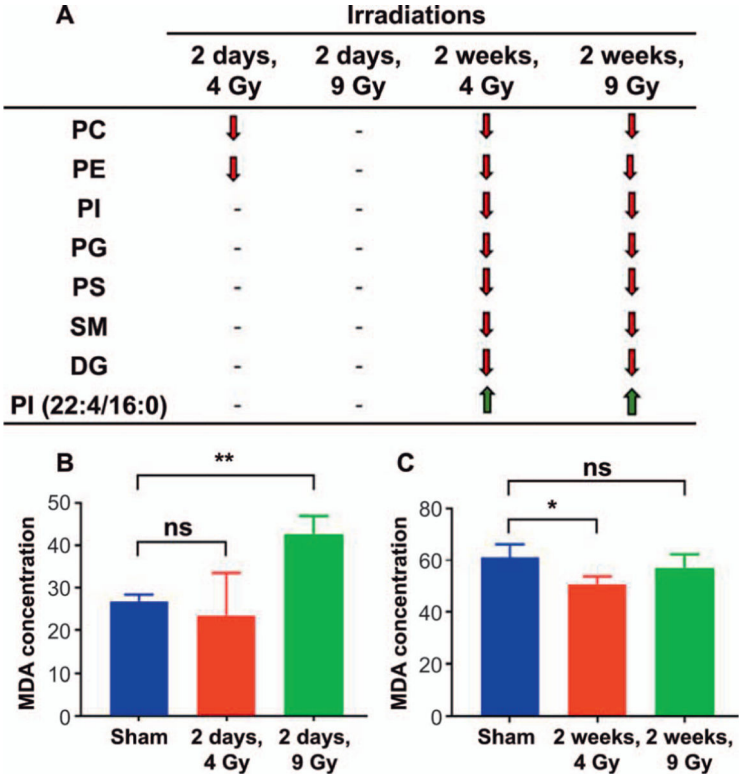

FIG. 3.

Dyslipidemia and increased lipid peroxidation in irradiated mice. Panel A: Representative overview of validated classes of lipids that were significantly dysregulated ($P < 0.05$, fold change <0.5 or >1.8) in hippocampal tissue of mice receiving either 4 Gy whole-body or 9 Gy cranial irradiation compared to sham-irradiated controls. Tissue was harvested at either two days or two weeks postirradiation. One outlier, PI (22:4/16:0), was significantly upregulated in both two-week radiation cohorts. The biological significance of this lipid is still under investigation. Panel B: Graphical representation of lipid peroxidation assay performed on mouse hippocampal tissue at two days and (panel C) two weeks postirradiation. MDA concentration is μ*M*/μg of protein. Experiments were performed in triplicate. Two-tailed *t* test with equal variance was used to calculate significance. *$P < 0.05$, **$P < 0.01$. PC = phosphatidylcholines; PE = phosphatidyl-ethanolamines; PI = phosphatidylinositols; PG = phosphatidylglycerols; PS = phosphatidylserines; SM = sphingomyelins; DG = diacylglycerols.

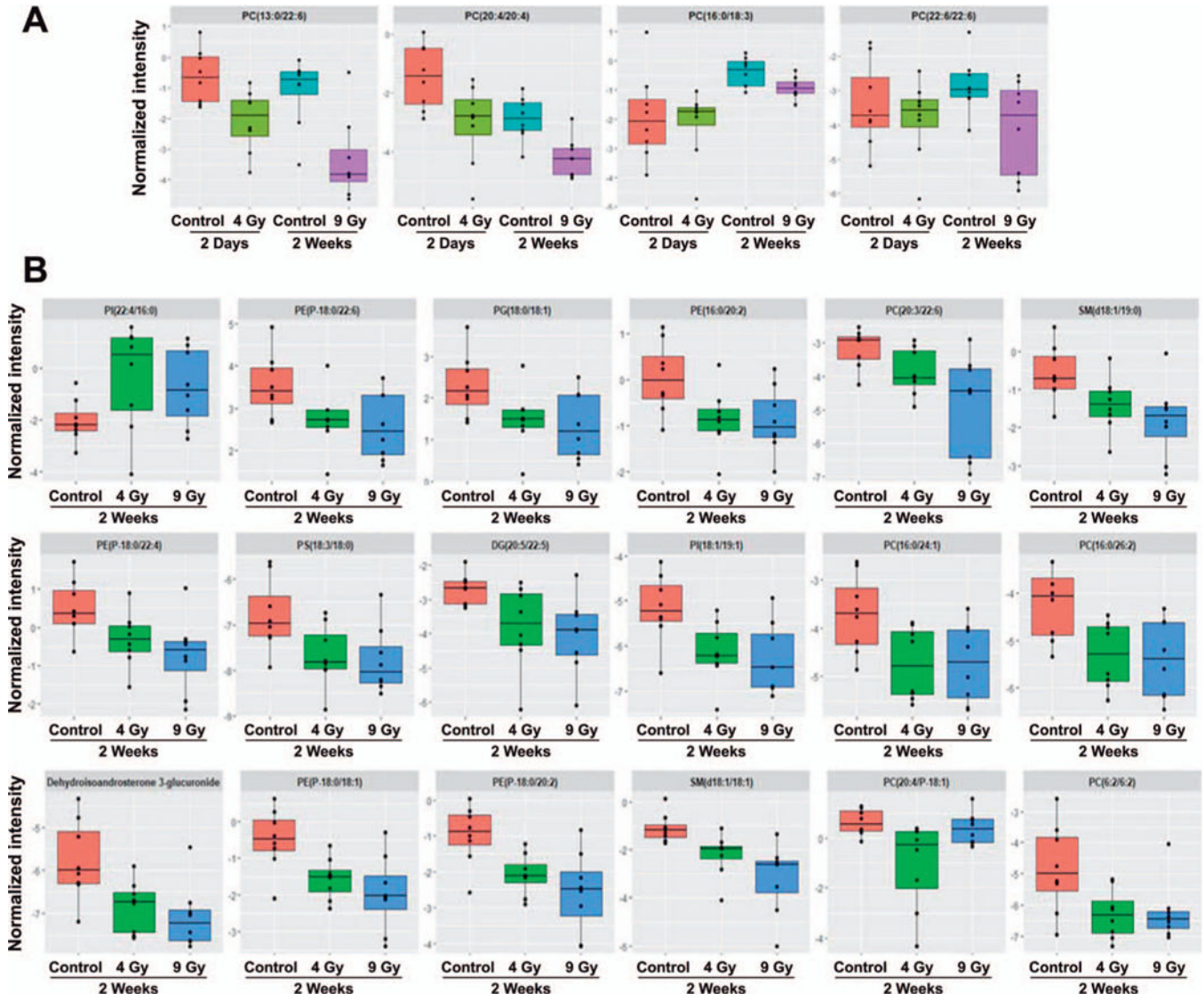

FIG. 4.

Whole-body irradiation at 4 Gy shapes hippocampal tissue-level metabolite profile in a fashion similar to 9 Gy cranial localized irradiation. Box and whisker plots of shared metabolites were validated in (panel A) two-day 4 Gy whole-body and two-week 9 Gy cranially irradiated mouse cohorts, and (panel B) 4 Gy whole-body and 9 Gy cranially irradiated mice (both cohorts at two weeks postirradiation). All values normalized to controls with majority of levels below 0, indicating fold reduction.

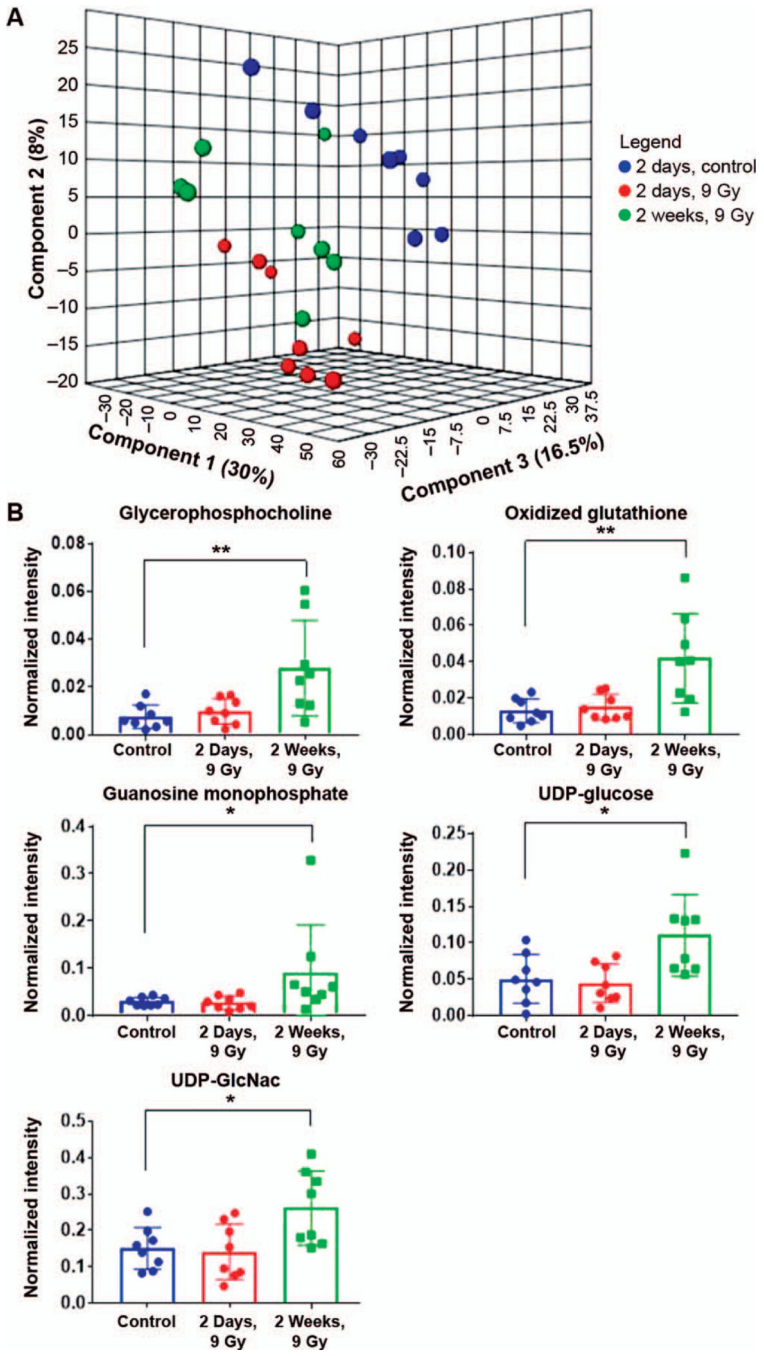

FIG. 5.

Comparative metabolites in two-week 9 Gy cranial localized irradiated mice. Panel A: PLS-DA plot visualizing metabolite profiles in hippocampal tissue derived from sham-irradiated mice vs. 9 Gy cranial irradiated mice after two days and two weeks. Representative data were captured in the metabolomics positive ionization mode. Panel B: Unique biomarkers validated in two-week 9 Gy cranial localized irradiated mice. $*P < 0.05$, $**P < 0.01$.

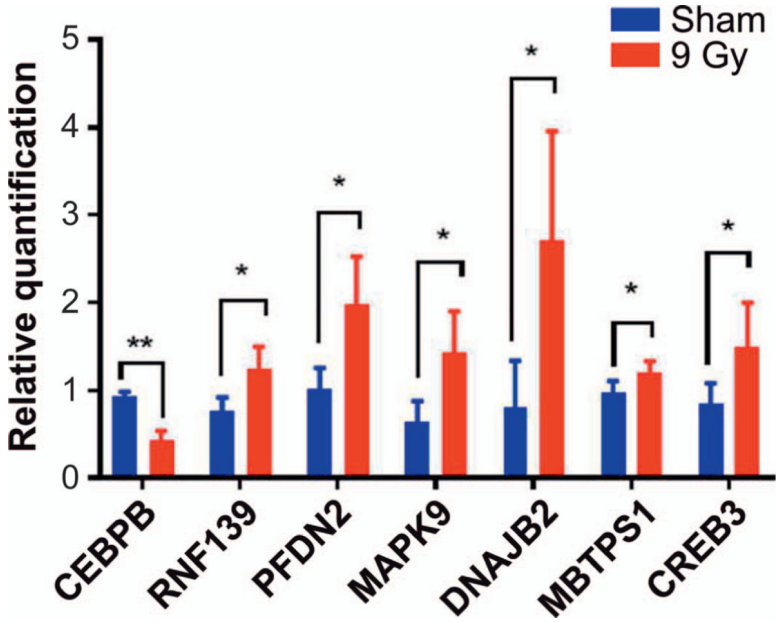

FIG. 6.

Cranial localized 9 Gy irradiation induces ER stress in mouse hippocampal tissue within two weeks after irradiation. Graphical representation of RT-qPCR data from homogenized mouse hippocampal tissue demonstrating significant dysregulation in genes associated with endoplasmic stress. n = 4 mice per group. All experiments were performed in triplicate. Relative quantification was performed using the ΔΔCt method, and Student's *t* test was used to determine significant gene expression changes between biological groups, with $P < 0.05$ considered significant. *$P < 0.05$, **$P < 0.01$.

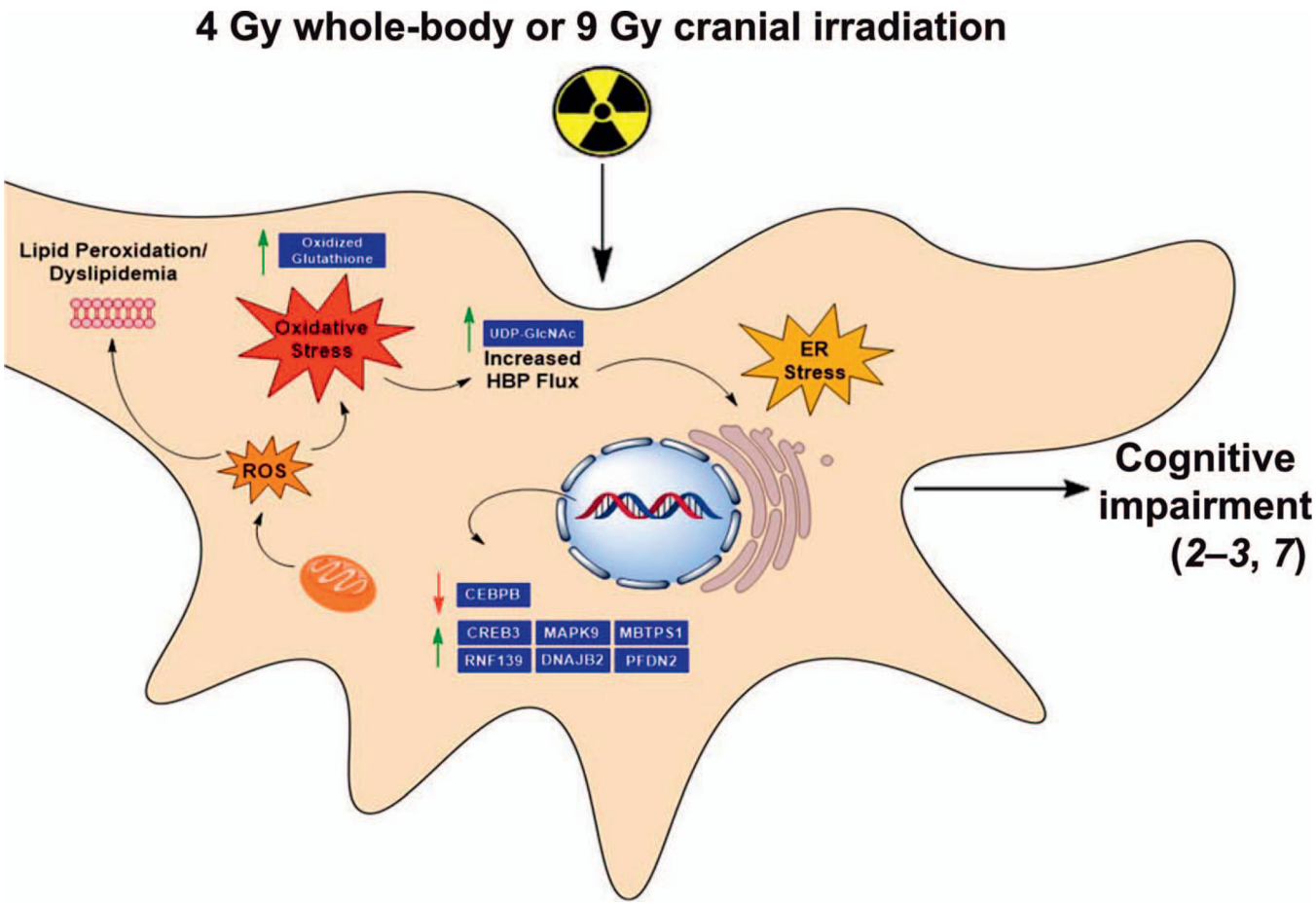

FIG. 7.

Proposed model for radiation-induced cognitive impairment. Whole-body X-ray irradiation (4 Gy) resulted in increased dyslipidemia, lipid peroxidation and oxidative stress. Cranial irradiation (9 Gy) resulted in increased dyslipidemia, oxidative stress, increased HBP flux and ER stress. Together, these biochemical changes could serve as early indicators of neurocognitive decline due to radiation exposure.